

Latency-Constrained Highly-Reliable mmWave Communication via Multi-point Connectivity

Dileep Kumar, *Student Member, IEEE*, Satya Joshi, *Member, IEEE*, and Antti Tölli, *Senior Member, IEEE*

Abstract—The sensitivity of millimeter-wave (mmWave) radio channel to blockage is a fundamental challenge in achieving low-latency and ultra-reliable connectivity. In this paper, we explore the viability of using coordinated multi-point (CoMP) transmission for a delay bounded and reliable mmWave communication. We propose a novel blockage-aware algorithm for the sum-power minimization problem under the user-specific latency requirements in a dynamic mobile access network. We use the Lyapunov optimization framework, and provide a dynamic control algorithm, which efficiently transforms a time-average stochastic problem into a sequence of deterministic subproblems. A robust beamformer design is then proposed by exploiting the queue backlogs and channel information, that efficiently allocates the required radio and cooperation resources, and proactively leverages the multi-antenna spatial diversity according to the instantaneous needs of the users. Further, to adapt to the uncertainties of the mmWave channel, we consider a pessimistic estimate of the rates over link blockage combinations and an adaptive selection of the CoMP serving set from the available remote radio units (RRUs). Moreover, after the relaxation of coupled and non-convex constraints via the Fractional Program (FP) techniques, a low-complexity closed-form iterative algorithm is provided by solving a system of Karush-Kuhn-Tucker (KKT) optimality conditions. The simulation results manifest that, in the presence of random blockages, the proposed methods outperform the baseline scenarios and provide power-efficient, high-reliable, and low-latency mmWave communication.

Index Terms—Reliable communication, blockage, queue backlogs, sum-power minimization, coordinated multi-point, lyapunov and convex optimization, Karush-Kuhn-Tucker conditions.

I. INTRODUCTION

The millimeter-wave (mmWave) communication is one of the key enabling technology for 5th-generation (5G) and beyond cellular systems, which facilitates throughput-intensive and low-latency applications, such as Industrial Internet-of-Things (IIoT), factory automation, augmented reality, and autonomous driving [2]. However, the full exploitation of the large available bandwidth at mmWave frequencies, is mainly challenged by the sensitivity of directional radio links to the blockage, i.e., due to relatively higher penetration and path-losses. These lead to rapid degradation (i.e., strong dips) in the received signal strength, and thus results in intermittent connectivity [3], [4]. For example, a human blocker can obstruct the dominant links for hundred of milliseconds, and may lead

to disconnecting the ongoing communication session, which severely impacts the network's reliability [3], [4]. Moreover, adapting to unpredictable blockage demands critical latency and signalling overhead, i.e., searching for an unblocked direction to re-establish the communication link [5]. Therefore, unless being addressed properly, the blockage appears as the main bottleneck that hinders in achieving low-latency and reliable mmWave connectivity.

To tackle the mmWave radio channel uncertainties, the use of macro-diversity via Coordinated Multi-Point (CoMP) has gained great interest. In particular, the Joint Transmission (JT)-CoMP connectivity, where each user equipment (UE) is coherently served by multiple spatially distributed remote radio units (RRUs) [6], [7]. Further, CoMP schemes are also considered in recent 3rd Generation Partnership Project (3GPP) releases [8], and it is envisioned that the use of multi-antenna spatial redundancy via geographically separated transceivers will be of high importance in the mmWave based deployment scenarios. As a proof-of-concept, Qualcomm has recently implemented a CoMP testbed at mmWave frequencies [9], and empirically shown the coverage and capacity improvements via flexible deployments in IIoT and factory automation scenarios.

A. Prior Work

The CoMP transmission and reception are mainly employed to enhance the system throughput, generally for the cell-edge users due to adverse channel conditions (e.g., higher path-loss and interference from neighboring RRUs). The CoMP techniques, such as, JT, Coordinated Beamforming (CB) and Dynamic Point Selection (DPS) are standardized in 3GPP [8], and has been widely studied in past decade under the context of legacy 4G systems [10]–[12]. For example, in [12], it is shown that JT-CoMP increases the coverage by up to 24% for cell-edge users and 17% for general users compared to non-cooperative scenarios. Recent studies have also considered the CoMP schemes in the mmWave frequencies [13]–[16].

In [13], from extensive real-time measurements, the authors showed a significant coverage improvement by simultaneously serving a user with spatially distributed transmitters. The network coverage gain for the mmWave system with multi-point connectivity, in the presence of random blockages, was also confirmed in [14], [15] using stochastic geometry tools. The gains of macro-diversity for the achievable rate and outage probability were quantified in [16], and it shown that CoMP connectivity, at the minimum of four spatially distributed links, can provide up to 76% capacity gains. However, CoMP techniques were still devised with the sole scope of enhancing

This work was supported by the European Commission in the framework of the H2020-EUJ-02-2018 project under grant no. 815056 (5G-Enhance) and Academy of Finland under grants no. 318927 (6Genesis Flagship).

This article was presented in part at the IEEE Global Commun. Conf., Taipei, Taiwan, Dec. 2020 [1]. (*Corresponding author: Dileep Kumar*)

The authors are with Centre for Wireless Communications, University of Oulu, FIN-90014 Oulu, Finland. (e-mail: dileep.kumar@oulu.fi; satya.joshi@oulu.fi; antti.tolli@oulu.fi).

the capacity and coverage [13]–[16], that inadvertently ends up relegating the stringent latency and reliability requirements, which is industrial-grade critical IoT applications (e.g., the factory automation scenarios). A step towards this direction is introduced in [6], where we provide reliable transmission schemes in the presence of random blockages, by preemptively underestimating the achievable rates over the potential link blockage combinations. However, these algorithms are still designed for the static case, i.e., the resource allocation problem for a given instance is studied without taking into account network dynamics and stringent latency conditions. Hence, these algorithms are not always applicable for, e.g., long-term time-dependent dynamics network deployment scenarios, and for retaining stable connectivity while satisfying the user-specific latency requirements. Furthermore, in low-latency industrial automation applications, the cycle time is shorter than the fading channel coherence time, which rules out the viability of automatic repeat request (ARQ)-based techniques for, e.g., delay bounded critical IoT applications [17], [18].

Thus, the limitations of retransmission events and the difficulty of accurate estimation of random blocking events motivate us to develop highly-reliable latency-constrained transmission strategies for dynamic networks. Specifically, we investigate on, how to use queue backlogs and channel information at the transmitter to efficiently allocate the required radio and cooperation resources, and to proactively exploit the multi-antenna spatial diversity according to the instantaneous needs of the users for a dynamic mmWave access networks.

B. Contributions

We develop a robust downlink transmission strategy, tailored for a JT-CoMP based dynamic networks, satisfying the user-specific latency requirement while retaining stable and resilient connectivity under the uncertainties of mmWave radio channel. Specifically, we consider a time-average sum-power minimization problem subject to maximum allowable queue length constraint in the presence of random blockages. The long-term time-average stochastic problem is transformed into a sequence of deterministic and independent subproblems using the Lyapunov optimization [19]. The coupled and non-convex constraints are approximated with the sequence of convex subsets by using the Fractional Program (FP) techniques [20]. Further, the proposed FP based relaxations allow an efficient implementation of closed-form iterative beamformer design that enables tailored complexity and processing performance. The main contributions of this paper are summarized as follow:

- A robust transmit beamformer design is proposed by utilizing the multi-antenna spatial diversity and geographically separated transceivers in CoMP connectivity scenarios. The time-average sum-power is minimized while ensuring the latency requirements, where, for each user, a pessimistic estimate of the rates overall possible subset combinations of potentially blocked links is considered [6]. Thus, managing mutually coupled link blocked combinations is more challenging than conventional constrained optimization.
- To adapt with the uncertainties of the mmWave radio channel, a proactive and dynamic selection of the CoMP

serving set from the available RRUs is proposed, e.g., by exploiting the queue backlogs and channel information. This preemptive rate estimate and dynamic modeling of the serving subset is shown to greatly improve the reliability and average sum-power performance while ensuring the user-specific latency requirement.

- After the relaxation of coupled and non-convex constraints via the Fractional Program (FP) techniques, a low-complexity robust beamformer design framework with specific performance and convergence characteristics is proposed by solving a system of closed-form Karush-Kuhn-Tucker (KKT) optimality conditions and parallel update of beamforming vectors corresponding to the spatially distributed RRUs. This leads to practical and computationally efficient implementation for, e.g., hardware constrained IoT devices with limited processing capabilities in IIoT and factory automation scenarios.

The paper is an extended version of our previously published conference paper [1]. It is worth highlighting, in [6] we studied reliable downlink transmission schemes for Weighted Sum-Rate Maximization (WSRM) problem. However, the algorithms were designed without taking into account stringent user-specific latency requirements and network dynamics. Hence, these schemes are not applicable to latency constrained dynamic mobile access scenarios. Motivated by the above highlighted concerns, we explored the viability of using CoMP transmission for a delay bounded and reliable mmWave communication in [1]. Nevertheless, the beamformer designs in [1], [6] were still based on the well-known Successive Convex Approximation (SCA) framework [21]. Further, the pessimistic estimate of the achievable rates in [1], [6] were also modeled over the fixed subset combinations of serving set of RRUs, and that may lead to inefficient utilization of network resources. Compared to our previous works [1], [6], in this paper, we have included the following additional notable contributions that provide more complete coverage and analysis in dynamic mmWave access networks. Specifically, the core question this paper tries to answer is how to use queue backlogs and channel information at the transmitter to efficiently allocate the required radio and cooperation resources, and to proactively exploit multi-antenna spatial diversity according to the instantaneous needs of the users in dynamic mobile network conditions. Further, we extend the standard FP quadratic transform techniques [20], i.e., to take into consideration JT-CoMP connectivity and provide a novel grouping of a multitude of potentially coupled and non-convex SINR conditions, that raise from the link blockage subset combinations. The proposed extension facilitates a low-complexity iterative algorithm, where each step is computed in closed-form expressions. All of the aforementioned results have been further improved and extended in this paper while accounting network dynamics and link blockages. We provide comprehensive and detailed numerical examples to evaluate the performance advantage of the proposed solutions. Specifically, we quantify the underlying trade-offs in terms of average sum-power, achievable rates, and reliable connectivity, under the uncertainties of mmWave channel and random blockages.

C. Organization and Notations

The remainder of this paper is organized as follows. In Section II, we illustrate the system, blockage, and network queuing model, as well as, provide the formulation of the problem. Section III provides a dynamic control algorithm. In Section IV, we describe the proposed beamformer designs. Section V provides an algorithm for dynamic serving set selection and theoretical analysis of outage. The validation of our proposed methods with the numerical results are presented in Section VI, and conclusions are given in Section VII.

Notations: In the following, we denote vectors and matrices with boldface lowercase and uppercase letters, respectively. The inverse, conjugate transpose and transpose operation is represented with the superscript $(\cdot)^{-1}$, $(\cdot)^H$ and $(\cdot)^T$, respectively. Cardinality of a set \mathcal{X} is denoted with $|\mathcal{X}|$. The norm and the real part of a complex number is represented with $|\cdot|$ and $\Re\{\cdot\}$, respectively. Notation $\mathbb{C}^{M \times N}$ is a $M \times N$ matrix with elements in the complex field. $[\mathbf{a}]_n$ is the n th element of \mathbf{a} , and $(a)^+ \triangleq \max(0, a)$. Notation $\nabla_{\mathbf{x}} y(\mathbf{x})$ represent the gradient of $y(\cdot)$ with respect to \mathbf{x} .

II. SYSTEM MODEL

We consider a downlink transmission in a mmWave based cloud (or centralize) radio access network (C-RAN) architecture, where all RRUs are connected to the edge cloud by the fronthaul links, as illustrated in Fig. 1. Each RRU is equipped with N transmit antennas. We use $\mathcal{K} = \{1, 2, \dots, K\}$ to denote the set of all single antenna UEs (also regarded as IoT devices), and $\mathcal{B} = \{1, 2, \dots, B\}$ to denote the set of all RRUs. Further, the set of RRUs that serve k th UE is denoted by \mathcal{B}_k , such that $\mathcal{B}_k \subseteq \mathcal{B}$, $\forall k \in \mathcal{K}$. We assume JT-CoMP connectivity [7], where each user k receives a synchronous signal from its serving RRUs \mathcal{B}_k $\forall k$. We assume that the network operates in a time-slotted manner, and slots are normalized to an integer value, e.g., $t \in \{1, 2, \dots\}$. Further, we assume that all RRUs use the same time-frequency resources for data transmission.

Let $\mathbf{f}_{b,k}(t) \in \mathbb{C}^{N \times 1}$ denote the transmit beamforming vector from b th RRU to k th UE. Then, the received signal $y_k(t)$ at k th UE during time slot t can be expressed as

$$y_k(t) = \sum_{b \in \mathcal{B}_k} \mathbf{h}_{b,k}^H(t) \mathbf{f}_{b,k}(t) d_k(t) + \sum_{u \in \mathcal{K} \setminus k} \sum_{g \in \mathcal{B}_u} \mathbf{h}_{g,u}^H(t) \mathbf{f}_{g,u}(t) d_u(t) + w_k(t), \quad (1)$$

where $\mathbf{h}_{b,k}(t) \in \mathbb{C}^{N \times 1}$ is the channel vector between RRU-UE pair (b, k) . Notation $d_k(t)$ is data symbol associated with k th UE, and $w_k(t) \in \mathcal{CN}(0, \sigma_k^2)$ is circularly symmetric additive white Gaussian noise (AWGN). Moreover, we assume that data symbols are normalized and independent, i.e., $\mathbb{E}\{|d_k(t)|^2\} = 1$ and $\mathbb{E}\{d_k(t) d_u^*(t)\} = 0$ for all $k, u \in \mathcal{K}$. The received signal-to-interference-plus-noise ratio (SINR) of k th UE during time slot t can be expressed as

$$\Gamma_k(\mathbf{F}(t)) = \frac{\left| \sum_{b \in \mathcal{B}_k} \mathbf{h}_{b,k}^H(t) \mathbf{f}_{b,k}(t) \right|^2}{\sigma_k^2 + \sum_{u \in \mathcal{K} \setminus k} \left| \sum_{g \in \mathcal{B}_u} \mathbf{h}_{g,u}^H(t) \mathbf{f}_{g,u}(t) \right|^2}, \quad (2)$$

where $\mathbf{F}(t) \triangleq [\mathbf{f}_{1,1}(t), \mathbf{f}_{1,2}(t), \dots, \mathbf{f}_{B,K}(t)]$.

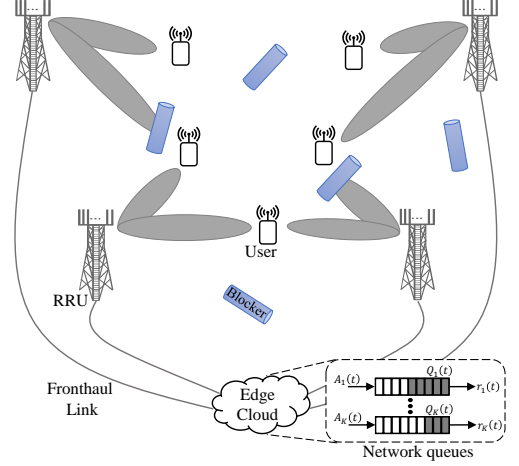


Fig. 1. C-RAN with network queues, B transmitters (RRUs) and K receivers (UEs) in the presence of randomly distributed blockers.

A. Blockage Model and Achievable Rate

In mmWave frequency band, the radio channel is spatially sparse due to low-scattering, reduced diffraction, and higher penetration and path losses [3], [4]. Hence, a mmWave communication link is inherently unreliable due to its susceptibility to blockages. The channel measurements in a typical mmWave outdoor scenarios have empirically shown that a link outage occurs with 20% – 60% probability [3], and may lead to a 10-fold decrease in the achievable sum-rate performance [4]. Therefore, unless being addressed properly, the random link blockage appears as the main bottleneck hindering the full exploitation of the mmWave radio channel. Thus, to characterize the aforementioned uncertainties of the mmWave channel, we consider a probabilistic binary blockage model [22], [23]. Specifically, the radio channel $\mathbf{h}_{b,k}(t)$ between RRU-UE pair (b, k) can have one of two states, i.e., it is either fully-available or completely blocked. Furthermore, we consider link specific blockage, and the blocking of channel $\{\mathbf{h}_{b,k} = \mathbf{0}\}_{b \in \mathcal{B}, k \in \mathcal{K}}$ for all t is independent. The methodology can easily be extended to more elaborate channel blocking models, e.g., by considering the distance and the spatio-temporal correlations [24]. In fact, this is an interesting topic for future extensions.

Similarly to [6], for improving system reliability and avoid outage under the uncertainties of mmWave channel, we preemptively underestimate the achievable SINR assuming that a portion of CoMP links would be blocked during the downlink data transmission phase. This is specifically required in the mmWave communication because of dynamic blockages, which are, in general, not possible to track during the channel estimation phase. Let baseband processing unit (BBU) assume that each user k have at least $L_k(t) \in [1, |\mathcal{B}_k|]$ available links (i.e., unblocked RRUs). Then, we allow BBU to proactively model the lower-bound of achievable SINR over all possible subset combinations, e.g., by excluding the potentially blocked links, and allocate the pessimistic rate to users. As an example, let the set of RRUs that are used to serve k th UE with RRU indices $\mathcal{B}_k = \{1, 2, 3\}$. Then, with the assumption of at least $L_k(t) = 2$ available links, the serving set of unblocked RRUs available to k th UE can be any one of following combinations:

$$\hat{\mathcal{B}}_k(L_k(t)) = \{\{1, 2\}, \{1, 3\}, \{2, 3\}, \{1, 2, 3\}\}. \quad (3)$$

Let $C(L_k(t))$ denote the cardinality of set $\widehat{\mathcal{B}}_k(L_k(t))$, defined as $C(L_k(t)) = \sum_{l=L_k(t)}^{|\mathcal{B}_k|} \frac{|\mathcal{B}_k|!}{l!(|\mathcal{B}_k|-l)!}$. We use \mathcal{B}_k^c to represent the c -th subset of $\widehat{\mathcal{B}}_k(L_k(t))$, i.e., subset $\mathcal{B}_k^c \in \widehat{\mathcal{B}}_k(L_k(t))$ such that cardinality $|\mathcal{B}_k^c| \geq L_k(t)$ for all $c = 1, \dots, C(L_k(t))$ during time slot t . Then, the received SINR of k th UE for \mathcal{B}_k^c (i.e., c -th subset) is obtained by excluding the potentially blocked RRUs in expression (2), and it can be expressed as

$$\Gamma_k(\mathbf{F}(t), \mathcal{B}_k^c) = \frac{\left| \sum_{b \in \mathcal{B}_k^c} \mathbf{h}_{b,k}^H(t) \mathbf{f}_{b,k}(t) \right|^2}{\sigma_k^2 + \sum_{u \in \mathcal{K} \setminus k} \left| \sum_{g \in \mathcal{B}_u \setminus \mathcal{D}_k^c} \mathbf{h}_{g,k}^H(t) \mathbf{f}_{g,u}(t) \right|^2}, \quad (4)$$

where $\mathcal{D}_k^c = \mathcal{B}_k \setminus \mathcal{B}_k^c$ denotes a subset of potentially blocked RRUs which are excluded from the interfering links to k th UE. Thus, the pessimistic achievable rate¹ for k th UE during time slot t can be expressed as

$$r_k(t) = \log_2(1 + \gamma_k(t)), \quad (5)$$

where $\gamma_k(t) = \min_c (\Gamma_k(\mathbf{F}(t), \mathcal{B}_k^c))$, $\forall c = 1, \dots, C(L_k(t))$, $\forall k$. In practice, the adverse channel condition and signaling overhead limits the maximum number of cooperating RRUs for each user (i.e., $\mathcal{B}_k \forall k$) [25]. Thus, the subset combinations $C(L_k(t))$ are fairly small for modestly sized systems [6].

It should be noted that each UE k still coherently receives the signal from all \mathcal{B}_k , unless RRUs are not available during the downlink data transmission phase due to random blockage. However, the actual RRUs available to serve k th UE cannot be known a priori in the dynamic blockage environment. Therefore, to maintain a reliable connectivity at each time slot, BBU preemptively underestimate the achievable SINR over all possible subset combinations $\mathcal{B}_k^c \in \widehat{\mathcal{B}}_k(L_k(t))$, which is associated with the design parameter $L_k(t) \forall k$, as it will become clear in Section V.

B. Network Queueing Model

We assume that the BBU maintains a set of internal queues for storing network layer data of all UEs [19, Ch. 5]. Let $Q_k(t)$ denote the current queue backlog of k th UE during time slot t , and $A_k(t)$ represents the amount of data that exogenously arrive to it, with the mean arrival rate of $\mathbb{E}[A_k(t)] = \lambda_k$. Then the dynamics of queue $Q_k(t)$ can be expressed as

$$Q_k(t+1) = [Q_k(t) - r_k(t) + A_k(t)]^+, \quad \forall k \in \mathcal{K}, \quad (6)$$

where $r_k(t)$ is transmission rate defined in expression (5). Furthermore, let \overline{Q}_k denote the time-averaged queue associated with k th UE, defined as

$$\overline{Q}_k \triangleq \lim_{T \rightarrow \infty} \frac{1}{T} \sum_{t=0}^{T-1} \mathbb{E}[Q_k(t)], \quad (7)$$

where the expectation depends on the control policy, and is with respect to the random channel states and arrivals.

According to the Little's law, the average delay is directly proportional to the average queue length \overline{Q}_k [26, Ch. 1.4]. Hence, for k th UE, we can achieve the desired latency

¹We consider Gaussian signalling and each UE decodes its intended signal by treating all other interfering signals as noise (4).

requirements by imposing a constraint on its queue length at each time slot. Here, we use a probabilistic constraint on the queue length, which is defined as

$$\Pr\{Q_k(t) \geq Q_k^{\text{th}}\} \leq \epsilon, \quad \forall t, \quad (8)$$

where Q_k^{th} is the maximum allowable queue length for k th UE and $\epsilon \ll 1$ is the tolerable queue length violation probability.

C. Problem Formulation

Our objective is to develop a power-efficient and reliable downlink transmission strategy for C-RAN based dynamic mmWave system, while satisfying the user-specific latency requirements. Specifically, we consider a problem of time-average sum-power minimization for mmWave communication with random channel blockages, subject to the maximum allowable queue length constraint for each UE, expressed as

$$\min_{\mathbf{F}(t), \gamma_k(t), \forall t} \lim_{T \rightarrow \infty} \frac{1}{T} \sum_{t=0}^{T-1} \left(\sum_{b \in \mathcal{B}} \sum_{k \in \mathcal{K}} \mathbb{E}[\|\mathbf{f}_{b,k}(t)\|^2] \right) \quad (9a)$$

$$\text{s.t.} \quad \Pr\{Q_k(t) \geq Q_k^{\text{th}}\} \leq \epsilon, \quad \forall k \in \mathcal{K}, \quad \forall t \quad (9b)$$

$$\gamma_k(t) = \min_c (\Gamma_k(\mathbf{F}(t), \mathcal{B}_k^c)), \quad (9c)$$

$$\forall c = 1, \dots, C(L_k(t)), \quad \forall k \in \mathcal{K}, \quad \forall t,$$

where the function $\Gamma_k(\mathbf{F}(t), \mathcal{B}_k^c)$ is defined in (4). The constraint (9b) ensures that the queue backlog of each user is less than Q_k^{th} at each time slot with the probability $1 - \epsilon$, and thus ensures the desired probabilistic latency requirements. Note that for each user k , the constraint (9c) is a pessimistic estimate of achievable SINR. More specifically, for a given parameter $L_k(t)$, BBU models the SINR of k th UE over all possible subset combinations of potentially available RRUs \mathcal{B}_k^c from the serving set $\widehat{\mathcal{B}}_k(L_k(t))$ (see Section II-A). Then, we allow BBU to proactively use the pessimistic estimate of SINR in order to allocate the downlink rate for the users such that transmission reliability is improved (i.e., to minimize the outage due to random blockages that appear during the transmission phase).

III. DYNAMIC ALGORITHM VIA LYAPUNOV OPTIMIZATION

The problem (9) is intractable as it consists of a long-term time-average sum-power objective function (9a), non-linear probabilistic queue length constraint (9b), and a large number of coupled non-convex SINR expressions (9c). In this section, we handle the first two sources of intractability, and derive a dynamic control algorithm for (9) by using the Lyapunov optimization technique [19]. The proposed convex relaxation via FP techniques and the closed-form iterative algorithms are then provided in Section IV.

We start by transforming the probabilistic queue length constraint (9b) into a time-average constraint using the Markov's inequality, i.e., $\Pr\{Q_k \geq Q_k^{\text{th}}\} \leq \mathbb{E}[Q_k]/Q_k^{\text{th}}$, $\forall k$ [26]. Thereby, problem (9) can be rewritten as

$$\min_{\mathbf{F}(t), \gamma_k(t), \forall t} \lim_{T \rightarrow \infty} \frac{1}{T} \sum_{t=0}^{T-1} \left(\sum_{b \in \mathcal{B}} \sum_{k \in \mathcal{K}} \mathbb{E}[\|\mathbf{f}_{b,k}(t)\|^2] \right) \quad (10a)$$

$$\text{s.t.} \quad \lim_{T \rightarrow \infty} \frac{1}{T} \sum_{t=0}^{T-1} \mathbb{E}[Q_k(t)] \leq \epsilon Q_k^{\text{th}}, \quad \forall k \in \mathcal{K}, \quad \forall t \quad (10b)$$

$$\gamma_k(t) \leq \Gamma_k(\mathbf{F}(t), \mathcal{B}_k^c), \quad (10c)$$

$$\forall c = 1, \dots, C(L_k(t)), \quad \forall k \in \mathcal{K}, \quad \forall t,$$

Note that we have relaxed (9c) while writing constraint (10c), and both these constraints are equivalent at the optimality.

Now, we use the Lyapunov optimization framework, specifically, a *drift-plus-penalty* method [19] to find a solution of problem (10). We enforce the long-term time-average constraint (10b) by transforming it into a queue stability problem [19, Ch. 5]. Specifically, a virtual queue associated with (10b) for each user k is introduced, and the stability of these virtual queue implies that the constraint (10b) is met.

Let $Z_k(t)$ be the virtual queue associated with (10b) for k th UE, and we update $Z_k(t)$ as

$$Z_k(t+1) = [Z_k(t) + Q_k(t+1) - \epsilon Q_k^{\text{th}}]^+, \quad \forall k \in \mathcal{K}. \quad (11)$$

The expression (11) can be interpreted as a queue dynamics for k th UE with arrival rate $Q_k(t+1)$ and service rate ϵQ_k^{th} . It can be observed from (11) that if the queue length of a user is larger than the delay tolerance, the virtual queue will increase. Therefore, if the virtual queues $\{Z_k(t)\}_{k \in \mathcal{K}}$ are stable, then by using [19, Theorem 2.5] we can show that (10b) is satisfied.

We now define Lyapunov function and its drift, which is used to stabilize queues $\{Z_k(t)\}_{k \in \mathcal{K}}$. For a compact representation, let $\Psi(t) = [Z_1(t), \dots, Z_K(t), Q_1(t), \dots, Q_K(t)]^T$ denote a collection of virtual and actual queues. Then we define following quadratic Lyapunov function:

$$\mathcal{L}(\Psi(t)) \triangleq \frac{1}{2} \sum_{k \in \mathcal{K}} Z_k(t)^2. \quad (12)$$

Intuitively, we can observe that if $\mathcal{L}(\Psi(t))$ is small, then all queues $\{Z_k(t)\}_{k \in \mathcal{K}}$ are small. Contrarily, if $\mathcal{L}(\Psi(t))$ is large then at least one of the queues is large. Thus, by minimizing a drift of $\mathcal{L}(\Psi(t))$ from one time slot to another, queues $\{Z_k(t)\}_{k \in \mathcal{K}}$ can be stabilized.

Then the Lyapunov drift [19, Ch. 5], which describes the change in network congestion between consecutive time slots, can be expressed as

$$\begin{aligned} \Delta(\Psi(t)) &= \mathbb{E}[\mathcal{L}(\Psi(t+1)) - \mathcal{L}(\Psi(t)) | \Psi(t)] \\ &= \frac{1}{2} \mathbb{E} \left[\sum_{k \in \mathcal{K}} (Z_k(t+1)^2 - Z_k(t)^2) | \Psi(t) \right]. \end{aligned} \quad (13)$$

Next, by using expressions (6) and (11) in (13), an upper bound of drift $\Delta(\Psi(t))$ can be expressed as²

$$\begin{aligned} \Delta(\Psi(t)) &\leq \zeta + \Phi(t) - \\ &\quad \mathbb{E} \left[\sum_{k \in \mathcal{K}} (Q_k(t) + A_k(t) + Z_k(t)) r_k(t) | \Psi(t) \right], \end{aligned} \quad (14)$$

where ζ and $\Phi(t)$ are positive constants, and satisfy the following condition³ for all time slots:

$$\begin{aligned} \zeta &\geq \frac{1}{2} \mathbb{E} \left[\sum_{k \in \mathcal{K}} A_k(t)^2 + r_k(t)^2 | \Psi(t) \right], \\ \Phi(t) &= \sum_{k \in \mathcal{K}} \left[\frac{1}{2} (\epsilon Q_k^{\text{th}})^2 + \frac{1}{2} Q_k(t)^2 \right. \\ &\quad \left. + Z_k(t) Q_k(t) + (Q_k(t) + Z_k(t)) A_k(t) \right]. \end{aligned}$$

²To obtain (14), we have used the fact that $([a+b-c]^+)^2 \leq (a+b-c)^2$ for any $a \geq 0$, $b \geq 0$, and $c \geq 0$.

³We have assumed that second moments of arrival and transmission processes are bounded [19]. The derivation is omitted due to lack of space, and we refer the reader to [19] for the details.

Now we define following *drift-plus-penalty* function [19] for problem (10):

$$\Delta(\Psi(t)) + V \mathbb{E} \left[\sum_{b \in \mathcal{B}} \sum_{k \in \mathcal{K}} \|\mathbf{f}_{b,k}(t)\|^2 | \Psi(t) \right], \quad (15)$$

where $V \geq 0$ is a trade-off parameter. By using expression (14) in (15), and minimizing the upper bound of (15) subject to constraint (10c) at each time slot, we can stabilize queues $\{Z_k(t)\}_{k \in \mathcal{K}}$ and minimize the sum power objective function of problem (10). Thus, we utilize the concept of *opportunistic minimization of an expectation* [19, Ch. 1.8] to minimize the drift-plus-penalty function (15), and obtain a dynamic control algorithm as detailed in Algorithm 1.

Algorithm 1: Dynamic control algorithm for (9)

- 1 For a given time slot t , observe current queue backlogs $\{Q_k(t), Z_k(t)\}$ and solve following problem:

$$\begin{aligned} \min_{\mathbf{F}(t), \gamma_k(t)} \quad & V \sum_{b \in \mathcal{B}} \sum_{k \in \mathcal{K}} \|\mathbf{f}_{b,k}(t)\|^2 - \sum_{k \in \mathcal{K}} (Q_k(t) \\ & + A_k(t) + Z_k(t)) \log_2(1 + \gamma_k(t)) \end{aligned} \quad (16a)$$

s.t. $\gamma_k(t) \leq \Gamma_k(\mathbf{F}(t), \mathcal{B}_k^c), \quad \forall c, \forall k \in \mathcal{K}. \quad (16b)$
 - 2 Update queues $Q_k(t+1)$ and $Z_k(t+1)$ by using (6) and (11), respectively, for all $k \in \mathcal{K}$
 - 3 Set $t = t + 1$, and go to step 1
-

At each time slot of Algorithm 1, we need to solve problem (16) to find optimal beamforming vectors $\mathbf{F}(t)$. Therefore, we derive iterative algorithms for this in the next section.

IV. ITERATIVE ALGORITHMS FOR PROBLEM (16)

The problem (16) is intractable as-is, mainly due to coupled and non-convex SINR expressions (16b). In this section, we elaborate on finding the solution of problem (16) by using the FP quadratic transform techniques [20]. In addition, we also provide a low-complexity beamformer design via iterative evaluation of the closed-form KKT optimality conditions and by the parallel update of beamformers corresponding to the spatially distributed RRs.

It is worth highlighting, in the FP techniques [20], [27], [28], all non-convex constraints are approximated with the sequence of convex subset, and the underlying convex subproblem is then iteratively solved until the convergence of objective function to a local solution. The FP quadratic transform based solutions have been widely used in many applications, e.g., power control, energy efficiency, and multi-antenna interference coordination [20], [27], [28]. For example, the SINR relaxation via FP techniques is provided for downlink in [20, Section IV], [28, Section III] and for uplink in [27, Section V], assuming perfect CSI and no blockages. Further, all these algorithms are studied for the static case (i.e., the resource allocation problem for a given instance is studied). In view of the prior works, there lacks a systemic approach for the design of beamforming vectors in the JT-CoMP scenarios, while accounting for the uncertainties of mmWave radio channel in a time-average dynamic network with the stringent user-specific latency and reliability requirements, thus motivating the current work.

A. Solution via Fractional Program (FP) techniques

We start by using the expression of $\Gamma_k(\mathbf{F}, \mathcal{B}_k^c)$ (see (4)), and compactly rewrite (16b) as

$$\gamma_k(t) \leq \frac{|\mathbf{h}_k^{\text{cH}}(t)\mathbf{f}_k(t)|^2}{\sigma_k^2 + \sum_{u \in \mathcal{K} \setminus k} |\mathbf{h}_k^{\text{cH}}(t)\mathbf{f}_u(t)|^2}, \quad (17)$$

where $\mathbf{f}_k(t) \triangleq [\mathbb{1}_{\mathcal{B}_k}(1)\mathbf{f}_{1,k}^T(t), \dots, \mathbb{1}_{\mathcal{B}_k}(B)\mathbf{f}_{B,k}^T(t)]^T \in \mathbb{C}^{|\mathcal{B}|N \times 1}$ and $\mathbf{h}_k^c(t) \triangleq [\mathbb{1}_{\mathcal{G}_k^c}(1)\mathbf{h}_{1,k}^T(t), \dots, \mathbb{1}_{\mathcal{G}_k^c}(B)\mathbf{h}_{B,k}^T(t)]^T \in \mathbb{C}^{|\mathcal{B}|N \times 1}$ denotes the stacked beamformer and channel, respectively. The indicator function $\mathbb{1}_{\mathcal{G}_k^c}(b)$ and $\mathbb{1}_{\mathcal{B}_j}(b)$ are defined as

$$\begin{aligned} \mathbb{1}_{\mathcal{B}_k}(b) &= \begin{cases} 1 & \text{if and only if } b \in \mathcal{B}_k \\ 0 & \text{otherwise.} \end{cases} \\ \mathbb{1}_{\mathcal{G}_k^c}(b) &= \begin{cases} 1 & \text{if and only if } b \in \mathcal{B} \setminus \mathcal{D}_k^c \\ 0 & \text{otherwise,} \end{cases} \end{aligned}$$

where $\mathcal{G}_k^c = \mathcal{B} \setminus \mathcal{D}_k^c$ for all $c = 1, \dots, C(L_k)$ and $k \in \mathcal{K}$. In this section, we omit time index t to simplify the notation.

Let us now examine the characteristic of the objective function in problem (16). We can observe that the right-hand-side (RHS) of (16b) is a typical function of multiple fractional parameters (i.e., SINR expressions (17)). Thus, problem (16) can be recast as a multi-ratio fractional program problem. Motivated by the findings in [20], here we adopt the recently proposed FP quadratic transform techniques, wherein the non-convex problem is recast as a sequence of convex subproblem, and then iteratively solved until the convergence of objective function. We extend the approaches [20] to take into consideration coherent multi-point transmission and provide a novel grouping of a multitude of potentially coupled and non-convex SINR conditions, that raise from the link blockage subset combinations. We develop the following proposition based on the FP techniques [20, Theorem 1].

Proposition 1. The fractional terms in RHS of (17)

$$\frac{|\mathbf{h}_k^{\text{cH}}\mathbf{f}_k|^2}{\sigma_k^2 + \sum_{u \in \mathcal{K} \setminus k} |\mathbf{h}_k^{\text{cH}}\mathbf{f}_u|^2}, \quad (18)$$

is equivalent to

$$2\Re\{\nu_{k,c}^* \mathbf{h}_k^{\text{cH}}\mathbf{f}_k\} - \nu_{k,c}^* \left[\sigma_k^2 + \sum_{u \in \mathcal{K} \setminus k} |\mathbf{h}_k^{\text{cH}}\mathbf{f}_u|^2 \right] \nu_{k,c}, \quad (19)$$

when the auxiliary variable $\{\nu_{k,c}\}$ has the optimal value as

$$\nu_{k,c}^{(*)} = \frac{\mathbf{h}_k^{\text{cH}}\mathbf{f}_k}{\sigma_k^2 + \sum_{u \in \mathcal{K} \setminus k} |\mathbf{h}_k^{\text{cH}}\mathbf{f}_u|^2}, \quad (20)$$

for all $c = 1, \dots, C(L_k)$ and $k \in \mathcal{K}$. We refer the reader to [20] for details. Specifically, the Proposition 1 can be proved by following the steps in [20, Section IV].

Thereby using Proposition 1, we can obtain a solution for problem (16) by iteratively solving a sequence of convex subproblems [20]. For example, the convex subproblem for

i -th iteration along with corresponding dual variables can be expressed as

$$\min_{\mathbf{F}, \gamma_k} V \sum_{k \in \mathcal{K}} \|\mathbf{f}_k\|^2 - \sum_{k \in \mathcal{K}} (Q_k + A_k + Z_k) \log_2(1 + \gamma_k) \quad (21a)$$

$$\begin{aligned} e_{k,c} : \gamma_k &\leq 2\Re\{\nu_{k,c}^{*(i-1)} \mathbf{h}_k^{\text{cH}}\mathbf{f}_k\} - \nu_{k,c}^{*(i-1)} \left[\sigma_k^2 + \right. \\ \text{s.t.} \quad &\left. \sum_{u \in \mathcal{K} \setminus k} |\mathbf{h}_k^{\text{cH}}\mathbf{f}_u|^2 \right] \nu_{k,c}^{(i-1)}, \quad \forall c, \forall k \in \mathcal{K}, \end{aligned} \quad (21b)$$

where $\{e_{k,c}\}$ are non-negative Lagrangian multipliers associated with constraints (21b). Note that (21) provides an approximate solution for (16) in the vicinity of a fixed operating point $\{\nu_{k,c}^{(i-1)}\}$. Specifically, for fixed auxiliary variables, we first optimize the primal optimization variables, and then update auxiliary variables with the current solution using expression (20). Thus, the proposed FP quadratic transform technique is based on an iterative optimization framework. However, the update rules of the auxiliary variables are given in a closed-form expression (20), and it is proven to attain the stationary point solution at each iteration [20], [27]. Hence, by iteratively solving (21) while updating the auxiliary variables $\{\nu_{k,c}^{(i)}\}$ with current solution, we can find a best solution for (16), using existing convex optimization toolboxes, such as CVX [29]. The beamformer design with the proposed FP relaxations has been summarized in Algorithm 2.

Algorithm 2: FP based algorithm for (16)

- 1 Set $i = 1$ and initialize with a feasible $\{\nu_{k,c}^{(0)}\}$, $\forall c, \forall k$
 - 2 **repeat**
 - 3 Solve (21) with $\{\nu_{k,c}^{(i-1)}\}$ and denote the local optimal values as $\{\mathbf{f}_k^{(i)}, \gamma_k^{(i)}\}$
 - 4 Obtain $\nu_{k,c}^{(i)}$ using (20) with updated $\{\mathbf{f}_k^{(i)}\}$
 - 5 Set $i = i + 1$
 - 6 **until** convergence or for fixed number of iterations;
-

1) Solution via KKT Conditions for Problem (21): We can observe that for fixed auxiliary variables $\{\nu_{k,c}\}$, each subproblem (21) is a convex problem with respect to variables $\{\mathbf{f}_k, \gamma_k\}$. Thus, we can efficiently obtain the solution by the Lagrangian multiplier method. Here, we tackle (21) by iteratively solving a system of KKT optimality conditions [30, Ch. 5.5], and, in general, it admits a closed-form solution that does not rely on generic convex solvers. The Lagrangian $\mathcal{L}_{\text{FP}}(\mathbf{F}, \gamma_k, \nu_{k,c}, e_{k,c})$ of problem (21) is given in (30). The stationary conditions for k th UE is obtained by differentiating (30) with respect to associated primal optimization variables $\{\mathbf{f}_k, \gamma_k\}$ for all $k \in \mathcal{K}$ (refer to [30, Ch. 5.5.3] for details). Thus, the stationary conditions of each user k for problem (21) can be expressed as

$$\nabla_{\gamma_k} : \sum_{c=1}^{C(L_k)} e_{k,c} = \frac{Q_k + A_k + Z_k}{1 + \gamma_k}, \quad (31a)$$

$$\begin{aligned} \nabla_{\mathbf{f}_k} : \sum_{c=1}^{C(L_k)} e_{k,c} \left(\nu_{k,c}^{*(i-1)} \mathbf{h}_k^{\text{cH}} \right) &= \mathbf{f}_k^H \left(V \mathbf{1} + \right. \\ &\left. \sum_{u \in \mathcal{K} \setminus k} \sum_{c=1}^{C(L_u)} e_{u,c} \nu_{u,c}^{*(i-1)} (\mathbf{h}_u^{\text{cH}} \mathbf{h}_u^{\text{cH}}) \nu_{u,c}^{(i-1)} \right). \end{aligned} \quad (31b)$$

$$\begin{aligned} \mathfrak{L}_{\text{FP}}(\mathbf{F}, \gamma_k, \nu_{k,c} e_{k,c}) = & \sum_{k=1}^K \left[V \|\mathbf{f}_k\|^2 - (Q_k + A_k + Z_k) \log_2(1 + \gamma_k) + \sum_{c=1}^{C(L_k)} e_{k,c} \gamma_k \right. \\ & \left. - 2 \sum_{c=1}^{C(L_k)} e_{k,c} \Re\{\nu_{k,c}^{*(i-1)} \mathbf{h}_k^{\text{cH}} \mathbf{f}_k\} + \sum_{c=1}^{C(L_k)} e_{k,c} |\nu_{k,c}^{(i-1)}|^2 \sigma_k^2 + \sum_{u \in \mathcal{K} \setminus k} \sum_{c=1}^{C(L_u)} e_{u,c} \nu_{u,c}^{*(i-1)} |\mathbf{h}_u^{\text{cH}} \mathbf{f}_k|^2 \nu_{u,c}^{(i-1)} \right]. \quad (30) \end{aligned}$$

In addition to (31) and primal-dual feasibility constraints, the KKT conditions also include the complementary slackness as

$$e_{k,c} \left\{ \gamma_k - 2 \Re\{\nu_{k,c}^{*(i-1)} \mathbf{h}_k^{\text{cH}} \mathbf{f}_k\} + \nu_{k,c}^{*(i-1)} \left[\sigma_k^2 + \sum_{u \in \mathcal{K} \setminus k} |\mathbf{h}_k^{\text{cH}} \mathbf{f}_u|^2 \right] \nu_{k,c}^{(i-1)} \right\} = 0, \quad \forall c, \forall k \in \mathcal{K}. \quad (32)$$

Note that, the user-specific SINR constraint (21b) is mutually coupled and interdependent over the serving set combinations (see Section II-A). Hence, obtaining a closed-form solution for the associated Lagrangian multipliers $\{e_{k,c}\}$ in expression (31) is considerably more difficult than the case with single and non-coupled QoS constraint for each user [7], [28]. Thus, to overcome this challenge, we resort to the subgradient approach, where all non-negative Lagrangian multipliers $\{e_{k,c}\}$ are iteratively solved using the subgradient method [31]. The closed-form steps in the iterative algorithm are:

$$\mathbf{f}_k^{(i)\text{H}} = \sum_{c=1}^{C(L_k)} e_{k,c}^{(i-1)} \left(\nu_{k,c}^{*(i-1)} \mathbf{h}_k^{\text{cH}} \right) \times \quad (33a)$$

$$\left\{ V \mathbf{1} + \sum_{u \in \mathcal{K} \setminus k} \sum_{c=1}^{C(L_u)} e_{u,c}^{(i-1)} \nu_{u,c}^{*(i-1)} (\mathbf{h}_u^{\text{cH}} \mathbf{h}_u) \nu_{u,c}^{(i-1)} \right\}^{-1},$$

$$\gamma_k^{(i)} = \frac{Q_k + A_k + Z_k}{\sum_{c=1}^{C(L_k)} e_{k,c}^{(i-1)}} - 1, \quad (33b)$$

$$\Gamma_k^{(i)}(\mathbf{F}, \mathcal{B}_k^c) = \frac{|\mathbf{h}_k^{\text{cH}} \mathbf{f}_k^{(i)}|^2}{\sigma_k^2 + \sum_{u \in \mathcal{K} \setminus k} |\mathbf{h}_k^{\text{cH}} \mathbf{f}_u^{(i)}|^2}, \quad (33c)$$

$$e_{k,c}^{(i)} = \left(e_{k,c}^{(i-1)} + \beta_e [\gamma_k^{(i)} - \text{expression (19)}] \right)^+, \quad (33d)$$

$$\nu_{k,c}^{(i)} = \frac{\mathbf{h}_k^{\text{cH}} \mathbf{f}_k^{(i)}}{\sigma_k^2 + \sum_{u \in \mathcal{K} \setminus k} |\mathbf{h}_k^{\text{cH}} \mathbf{f}_u^{(i)}|^2}. \quad (33e)$$

where β_e is small positive step-size⁴. In expression (33d), the dual variables $\{e_{k,c}\}$ are iteratively updated based on the violation of SINR constraint, e.g., the complementary slackness conditions (32), using the subgradient method [31]. The proposed beamformer design by solving a system of closed-form KKT expressions is summarized in Algorithm 3.

B. Feasible Initialization and Complexity Analysis

1) *Feasible Initialization*: In the FP methods, the non-convex constraints (16b) are approximated with the sequence of convex subsets, and then iteratively solved until the convergence of objective function to a stationary point solution. Thus, it is important to initialize the proposed iterative algorithms with a feasible starting point, as it impacts the

Algorithm 3: KKT based iterative algorithm for (21)

- 1 Set $i = 1$ and initialize $\{\nu_{k,c}^{(0)}\}, \forall c, \forall k$
- 2 **repeat**
- 3 Solve $\mathbf{f}_k^{(i)}$ from (33a) with $\{\nu_{k,c}^{(i-1)}, e_{k,c}^{(i-1)}\}$
- 4 Obtain $\gamma_k^{(i)}$ from (33b)
- 5 Calculate $\Gamma_k^{(i)}(\mathbf{F}, \mathcal{B}_k^c)$ from (33c) with updated $\{\mathbf{f}_k^{(i)}\}$
- 6 Obtain $e_{k,c}^{(i)}$ using (33d)
- 7 Solve $\nu_{k,c}^{(i)}$ from (33e) with updated $\{\mathbf{f}_k^{(i)}\}$
- 8 Set $i = i + 1$
- 9 **until** convergence or for fixed iterations;

problem feasibility and the rate of convergence [20], [27]. To this end, one possible option for a feasible $\{\mathbf{f}_k^{(0)}\}$ is to use any randomly generated beamforming vector. Then, compute the lower bound of achievable SINR from (4), i.e., $\gamma_k^{(0)} = \min_c (\Gamma_k(\mathcal{B}_k^c)), \forall c = 1, 2, \dots, C(L_k), \forall k \in \mathcal{K}$. Furthermore, with the feasible $\{\mathbf{f}_k^{(0)}\}$, the initial values of the auxiliary variables $\{\nu_{k,c}^{(0)}\}$ can be computed using (20). The non-negative Lagrangian multiplier $\{e_{k,c}^{(0)}\}$ in Algorithm 3 are initialized such that $\sum_{c=1}^{C(L_k)} e_{k,c}^{(0)} > 0$, e.g., at least one of the coupled SINR constraint is active for each user (see (31a) and (33b) for more details). It is worth noting that the initialization of the iterative Algorithms with different *feasible* initial values $\{\mathbf{f}_k^{(0)}, \gamma_k^{(0)}, \nu_{k,c}^{(0)}, e_{k,c}^{(0)}\}$, in general, does not impact the local solution of problem (16), provided a sufficient number of iterations [30]. For detail on the convergence and the stationary point solution, we refer the readers to [20], [27].

2) *Complexity Analysis*: The approximated convex subproblem (21) can be solved in a generic convex optimization solver, i.e., as a sequence of second-order cone programs (SOCP) [32]. The interior points methods are generally adopted to efficiently solve the SOCP formulations, wherein, the computational complexity of each iteration scales with the length of system wide joint beamforming vectors ($|\mathcal{B}|N$) and the number of constraints [32]. In this case, it can be shown that solving each subproblem (21) requires $\mathcal{O}((|\mathcal{B}|N)^{3.5})$ arithmetic operations. The computational complexity of the iterative algorithms, e.g., by solving a system of closed-form KKT optimality conditions, is mainly dominated by expression (33a) for each subproblem (21). We can observe that expression (33a) consists of matrix multiplications and inverse operations, and the computational complexity of each iteration scales with the length of RRU specific beamforming vector (N). Thus, it can be shown that solving each subproblem via iterative evaluation of KKT optimality conditions

⁴The step size depends on the system model, as it directly affects the convergence rate and controls the oscillation in the objective function [31].

require $\mathcal{O}(|\mathcal{B}_k|N^3)$ arithmetic operations. Thus, algorithms based on iterative evaluation of closed-form KKT optimality conditions provide a conveniently parallel structure for the beamformer design with relatively lower complexity compared to the joint beamformer optimization across all RRUs.

V. DYNAMIC SERVING SUBSET SELECTION

We assume that the blockers are randomly distributed and independent for each time slot. Further, the position of each blocker and/or blockage events can not be known during the downlink data transmission phase. Therefore, to improve system reliability under these uncertainties of mmWave radio channel, we preemptively underestimate the achievable rate of each user, assuming that a portion of CoMP links would be blocked during the data transmission phase (see Section II-A). Let BBU assume that each user k have at least $L_k(t)$ available links (i.e., unblocked RRUs). Then we allow BBU to proactively model the pessimistic estimate of SINR over all possible subset combinations, e.g., by excluding the potentially blocked links, and allocate the rate to users such that transmission reliability is improved (for more details see Section II-A). Hence, the user-specific CoMP subset combinations $L_k(t) \in [1, |\mathcal{B}_k|]$ $\forall k$ is a design parameter, which can be tuned for each time slot t , e.g., based on available queue backlogs and channel information, to achieve desired rate, reliability, and user-specific latency requirements.

Let $\varrho_k(t) \in [0, 1]$ denote the blockage probability of k th UE during time slot t . Then, for a fixed subset combinations $L_k(t)$, the success probability of k th UE can be approximated as (we refer the reader to [6, Section III] for details)

$$p_k(L_k(t)) = \sum_{l=0}^{|\mathcal{B}_k| - L_k(t)} \binom{|\mathcal{B}_k|}{l} (1 - \varrho_k(t))^{|\mathcal{B}_k| - l} (\varrho_k(t))^l. \quad (34)$$

Since all users are independent, the outage probability of k th UE can be expressed as

$$P_k^{\text{out}}(L_k(t)) = 1 - p_k(L_k(t)), \quad \forall k \in \mathcal{K}. \quad (35)$$

From expression (35), we can observe that the outage $P_k^{\text{out}}(L_k(t))$ is a monotonically increasing function of parameter $L_k(t)$. As an example, we can improve the system reliability and avoid the outage by preemptively assuming that a significant portion of the available CoMP RRUs (i.e., $|\mathcal{B}_k| - L_k(t)$, $\forall k$) are potentially blocked. However, this pessimistic assumption on available links may lead to a lower SINR estimate (see Section II-A), and hence, a lower rate to each user (5). Thus, to ensure the user-specific latency requirements (9b), the network consumes more power, and attempt to increase the instantaneous rate over the available subset of RRUs, \mathcal{B}_k^c $\forall k \in \mathcal{K}$.

Conversely, a less pessimistic assumption on subset size (i.e., a higher value of $L_k(t)$ $\forall k$) can provide higher instantaneous SINR (4), but it can be more susceptible to the outage, and results in less stable connectivity. Moreover, these outage events will eventually increase the queue-backlogs (6), i.e., due to unsuccessful downlink data transmissions. Thus, to guarantee the desired average latency requirements (9b), the network consumes more power, and tries to increase the

achievable rates in the following time slots. Clearly, there is a trade-off between reliable connectivity and sum-power performance, while ensuring the latency requirements.

Therefore, for each time slot t , first we need to choose parameter $L_k(t) \in [1, |\mathcal{B}_k|]$, and then solve problem (16) over a given subset combinations $C(L_k(t))$ for all $k \in \mathcal{K}$. Specifically, the parameter $L_k(t)$, such that the solution of problem (16) satisfy (9b) with the minimum sum-power is of our interest. Thus, we can observe that the constraint (9b) can be met with minimum sum-power, if the success probability of each user k satisfy $p_k(L_k(t)) \geq 1 - \epsilon$, $\forall k \in \mathcal{K}$. Hence, the parameter $L_k(t)$ for k th UE during time slot t can be computed by solving following:

$$\min_{L_k(t)} p_k(L_k(t)) \quad (36a)$$

$$\text{s.t. } p_k(L_k(t)) \geq 1 - \epsilon, \quad \forall L_k(t) \in [1, |\mathcal{B}_k|]. \quad (36b)$$

It should be noted that the blockage probability $\varrho_k(t)$ $\forall k$ is still an unknown parameter, and thus hinders solving (36). However, an approximation of blockage $\tilde{\varrho}_k(t)$ $\forall k$ can be obtained by, e.g., exploiting the available queue backlog information at the BBU. For example, in the considered C-RAN architecture, the centralized BBU is aware of the instantaneous arrivals, current queue backlogs, and channel information, for the design of beamforming vectors. Thus, user k during time slot t can be in outage, if the assigned downlink rates $r_k(t) \neq 0$ and the queue backlogs grow as $Q_k(t+1) = [Q_k(t) + A_k(t)]^+$, $\forall k \in \mathcal{K}$ (see expression (6) and (39) for details). Therefore, the outage of k th UE during time slot t can be approximated as

$$\mathbb{1}_{\mathcal{P}_k}(t) = \begin{cases} 1 & \text{if } \{r_k(t) \neq 0\} \cap \{Q_k(t+1) = [Q_k(t) + A_k(t)]^+\}, \\ 0 & \text{otherwise.} \end{cases}$$

where $\mathbb{1}_{\mathcal{P}_k}(t)$ is indicator function. Alternatively, the outage event can be (accurately) computed based on UE acknowledgments. However, in the presence of random link blockages, the mmWave feedback links are inherently unreliable and, hence, results in overestimation and increased delays [17], [18]. In fact, this is an interesting topic for future extensions. Thus, at each time slot t , BBU exploits the available channel and queue backlogs information of each user k to compute the approximated blockage as

$$\tilde{\varrho}_k(t) = \frac{1}{\delta_k} \sum_{i=t-\delta_k}^{t-1} \mathbb{1}_{\mathcal{P}_k}(i), \quad (37)$$

where δ_k is maximum averaging length. Hence, using the estimated time-averaged blocking, the BBU first computes the adequate size of the subset combinations from (36), and then solves problem (16) to obtain the beamforming vectors.

VI. SIMULATION RESULTS

This section provides numerical examples to quantify the performance advantage of the proposed algorithms. We consider a mmWave based donwlink transmission with UEs $K = 4$, RRUs $B = 4$, and each RRU is equipped with a uniform linear array (ULA) of $N = 16$ antennas. Further, RRUs are placed in a 50×50 meters square layout (resembling, e.g.,

a factory-type IIoT setup), and are connected to a common BBU in the edge cloud. All single antenna UEs are randomly dropped within the square, thus each UE has a different path-gain and angle with the RRUs.

The mmWave channel $\mathbf{h}_{b,k}(t)$ between a RRU-UE pair (b, k) is based on sparse geometric model [33], and defined as

$$\mathbf{h}_{b,k}(t) = \sqrt{\frac{N}{M}} \sum_{m=1}^M \omega_{b,k}(t) d_{b,k}^{-\psi_m(t)} \mathbf{a}_T(\phi_{b,k}^m(t)), \quad (38)$$

where M is the number of independent paths, which we set as $M = 3$, and $\omega_{b,k}(t)$ is random complex gain with zero mean and unit variance. The distance between RRU-UE pair is represented with $d_{b,k}$, and the notation ψ_m denote a random path-loss exponent. In the simulation, we consider $\psi_m(t) \in [2, 6]$, $\forall(m, t)$. The array response vector for ULA is represented with $\mathbf{a}_T(\phi_{b,k}^m(t)) \in \mathbb{C}^{N \times 1}$, and relative to the boresight of the RRU antenna array, the angle-of-departure (AoD) for each path is uniformly distributed, i.e., $\phi_{b,k}^m(t) \in [-\pi/2, \pi/2]$, $\forall(m, t)$. For simplicity, we assume a probabilistic blockage model [22], [23], where the radio channel between RRU-UE pair during downlink transmission phase, is either fully available, i.e., as in (38) or completely blocked, i.e., $\{\mathbf{h}_{b,k}(t) = \mathbf{0}\}$, with the probability of $q \in [0, 1]$ for all $b \in \mathcal{B}$ and $k \in \mathcal{K}$.

Recall that to improve the communication reliability and avoid outage under these uncertainties of mmWave radio channel, we use parameter $L_k (\leq |\mathcal{B}_k|)$ in problem (9), and proactively model the SINR over the link blockage combinations (see Section II-A). For simplicity, but without loss of generality, we assume identical parameters for each user k , i.e., serving set $|\mathcal{B}_k| = 4$, $L_k = L$, arrival $A_k \sim \text{Pois}(\lambda)$ with $\lambda = 3.5$ bits/slot and maximum queue length $Q_k^{\text{th}} = 5$ bits with tolerable probability $\epsilon = 0.1$ in problem (9) [1]. In the simulations, we set the frequency $f_c = 28$ GHz, the step size $\beta_e = 0.01$ in expression (33d).

The outage event occurs if the instantaneous transmit rate $r_k(t)$ exceeds the supported rate⁵ $c_k(t)$ for all $k \in \mathcal{K}$. Then, the queue dynamics $Q_k(t)$ in (6) can be expressed as

$$Q_k(t+1) = [Q_k(t) - r_k(t) \mathbb{1}_{\{r_k(t) \leq c_k(t)\}} + A_k(t)]^+, \quad \forall k, \quad (39)$$

where $\mathbb{1}_{\{\cdot\}}$ is an indicator function. Specifically, expression (39) implies that queue backlogs also increase with each unsuccessful downlink transmission due to random blockages. In our study, we will make use of subset size L to analyze the network performance. For the baseline methods, we consider CB (i.e., $|\mathcal{B}_k| = 1$, $\forall k$) [10] and full-JT (i.e., $L_k = |\mathcal{B}_k|$, $\forall k$) [7] based downlink beamformer designs.

A. Convergence Analysis

In Fig. 2, we examine the convergence behavior of proposed iterative algorithms for given randomly generated channel

⁵For a given time slot t , let $\mathcal{S}_k(t) = \{\gamma_k^*(t), \mathbf{f}_k^*(t)\}_{k \in \mathcal{K}}$ denote solution of problem (9). Then, for each user k , the transmission rate is given by $r_k(t) = \log_2(1 + \gamma_k^*(t))$. However, the actual supported rate (i.e., link capacity) for k th user depends on the obtained beamformers $\{\mathbf{f}_k^*(t)\}_{k \in \mathcal{K}}$ and current channel state $\{\mathbf{h}_{b,k}(t)\}_{b \in \mathcal{B}, k \in \mathcal{K}}$. However, channel can not be exactly known to the BBU during data transmission phase due to random blockages. Thus, the supported rate can be calculated using the actual SINR values (2), i.e., $c_k(t) = \log_2(1 + \Gamma_k(\mathbf{F}^*(t)))$, $\forall k$, and these rates are unknown to the BBU.

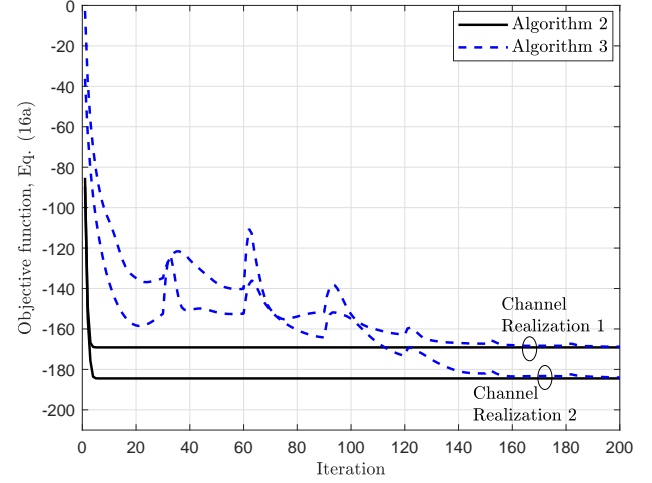


Fig. 2. Convergence performance of Algorithm 2 and Algorithm 3.

realizations. For simplicity but without loss of generality, we set parameters, $V = 1$, $L = 3$, and $q = 0$. Note that the solution of Algorithms 2 is obtained directly by using the convex optimization toolbox, SeDuMi [29]. In contrast, Algorithm 3 is solved from a system of closed-form KKT optimality conditions in an iterative manner (see (33)). We can observe that both algorithms converge to the same local solution, on average, within a fairly small number of iterations. It is worth highlighting, in general, the convergence of Algorithm 3 cannot be guaranteed to be monotonic due to subgradient updates (33d), and it can be tuned in accordance with the system parameters. We refer the reader to [31] on the convergence properties of the subgradient approach with different step size rules. The Algorithm 2 provides monotonic and faster convergence in terms of required approximation point updates. On the contrary, Algorithm 3 achieves comparable performance with a significant reduction in the per-iteration computational complexity, which can be useful for, e.g., hardware constrained IoT devices with limited processing capabilities in IIoT and factory automation scenarios.

B. Impact of the trade-off parameter V

First, in Fig. 3, we illustrate the latency performance with trade-off parameter $V = 1$ and blockage $q = 10\%$. The result shows that our proposed and baseline methods satisfy the maximum queue backlogs of each user k (i.e., $Q_k^{\text{th}} = 5$) within the allowable queue tolerance level $\epsilon = 0.1$. Thus, problem (9) is feasible, and the proposed convex relaxations still allow to achieve the desired user-specific latency requirements (i.e., constraint (9b) is met). However, our proposed beamformer designs, i.e., by considering a pessimistic estimate of rates over the subset combinations of potentially blocked CoMP RRUs, substantially improve the average sum-power performance, while ensuring the same latency requirements, as shown in Fig. 4. As an example, for the parameter $V = 1$ and $L = 2$, our proposed method improves the average sum-power performance by 8 dBm and 18 dBm compared to baseline CB and full-JT, respectively. Hence, the proposed methods significantly outperform the conventional full-JT [7] and CB [10]

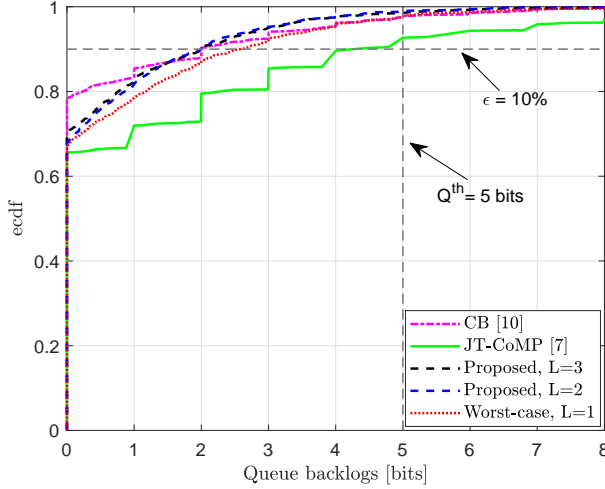


Fig. 3. Queue backlogs with $V = 1$ and blockage of 10%.

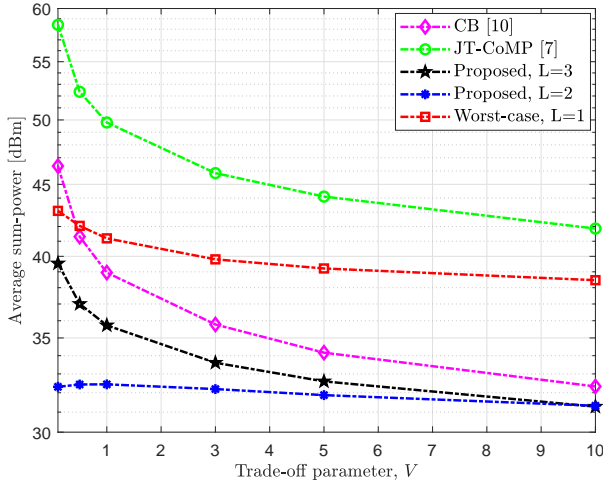


Fig. 4. Average sum-power with increasing V and blockage of 10%.

based downlink beamformer design, and thus provides power-efficient and low-latency mmWave communication.

Further, it can be observed from Fig. 4 that for a fixed queue length constraint, the average sum-power decreases with the increase in the value of trade-off parameter V . This behavior is expected, since higher values of parameter V linearly emphasize the minimization of the sum-power objective over the queue length, until the queue backlogs become substantially larger than the sum-power objective values (see (16a)).

Fig. 5 and Fig. 6 shows the evolution of the network queues $\{Q_k(t)\}$ and the associated virtual queues $\{Z_k(t)\}$ over time with the blockage $q = 10\%$ and the parameter $L = 3$, for user $k = 1$. Note that, we can observe similar behavior for all other users, but these are not included due to space limitations. It can be concluded from Fig. 5 that the queue backlogs increases differently for different values of trade-off parameters V , until it saturate and reaches a certain value (e.g., for $V = 10$ around $t = 115$ time slots), and then it oscillates, so as the constraint $\Pr\{Q_k(t) \geq Q_k^{\text{th}}\} \leq \epsilon$, is ensured, i.e., to achieve the average user-specific latency requirements. This is mainly because of the negative drift

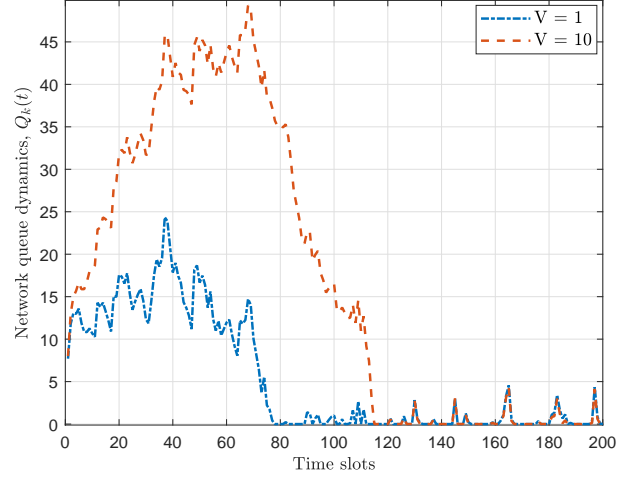


Fig. 5. Network queue dynamics with blockage of 10%.

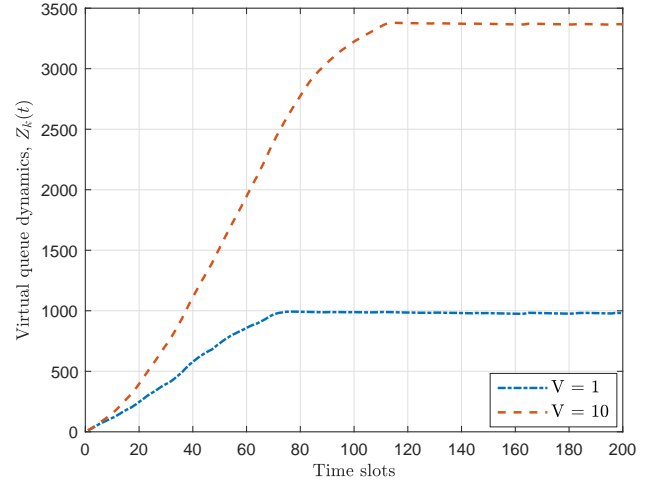


Fig. 6. Virtual queue dynamics with blockage of 10%.

property of the Lyapunov function [19, Ch. 4.4]. Thus, the stability of associated virtual queues $\{Z_k(t)\}$, i.e., as in Fig. 6, ensures that the network queues are bounded, and achieves the desired queue backlogs performance.

C. Dynamic selection of parameter L

Next, we investigate the dynamic selection of the serving set size, i.e., parameter $L(t)$ for each time slot t , which is obtained by solving (36). To do that, first in Fig. 7, we show the time-averaged blockage computed from expression (37) with the maximum averaging length $\delta_k = \min\{\tau, (t-1)\}$, and we set $\tau = 50$. It can be concluded that the estimate of the blockage in (37) closely matches with actual blockage probability, within a moderately small number of random channel realizations. Thus, expression (37) provides a fair approximation, and the resulting gap is mainly due to unpredictable random blockage events and uncertainties in the mmWave radio channel.

Further, it can be observed from Fig. 8 that the instantaneous choice of serving set size, i.e., to meet the success probability (36b), mainly depends on the accuracy of estimated block-

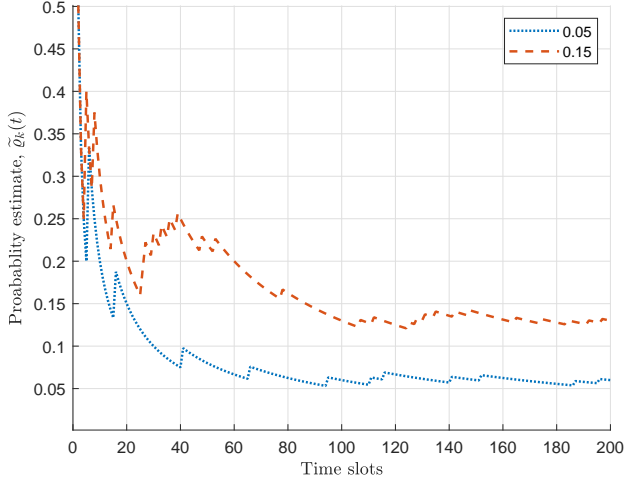


Fig. 7. Approximation of blockage probability using (37) .

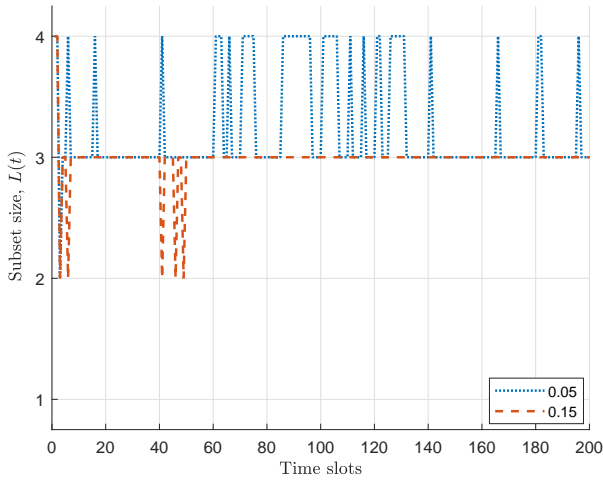


Fig. 8. Dynamic selection of subset size $L(t)$ by solving (36).

age. Furthermore, the oscillations in Fig. 8 is due to limited (and discrete) choices of parameter $L_k(t) \in [1, |\mathcal{B}_k|]$, $\forall k$, and possibly the minimum subset size satisfying (36b) can be in between these integer values. It is worth highlighting that the problem (36) aims at finding serving set size, such that solving problem (16) satisfy the (9b) with minimum sum-power. Therefore, large values of L may result in lower sum-power, but it may lead to higher outage, and thus it dynamically switches to a more pessimistic SINR estimate, i.e., to lower values of L , in the following time slot, to meet the average latency requirements. Hence, there is a trade-off between average sum-power, achievable rate, and reliability, as will be demonstrated in the following.

Fig. 9 illustrates the impact increasing blockage probability on constraint (9c) and sum-power performance. For example, the worst-case pessimistic assumption on available links (i.e., $L = 1$) leads to a lower SINR estimate. Thus, to ensure the user-specific latency requirements (9b), the network strives to increase the user's rate over the available subset of RRUs $\mathcal{B}_k^c \forall k \in \mathcal{K}$, i.e., by consuming higher network power. Thus, it results in relatively lower average sum-power performance, as

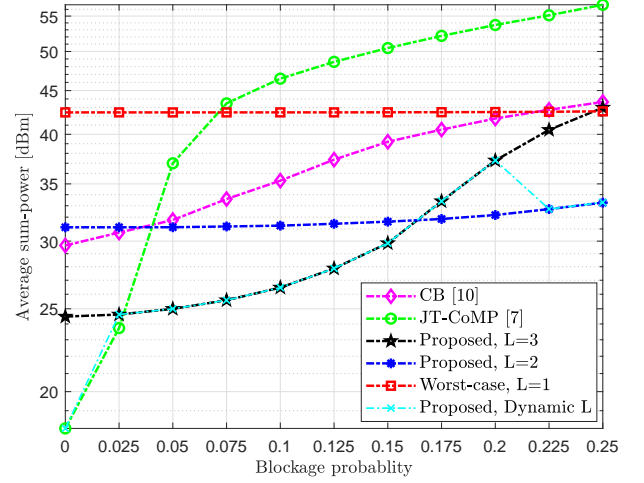


Fig. 9. Average sum-power with increasing blockage and $V = 1$.

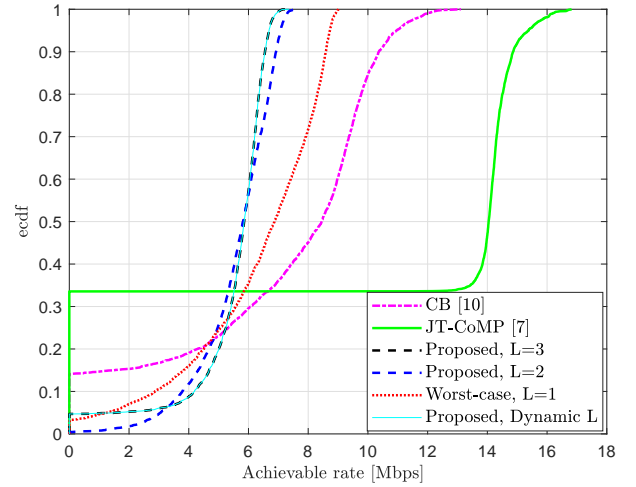


Fig. 10. Achievable user-rate with $V = 1$, blockage $q = 10\%$.

shown in Fig. 9. Conversely, a least pessimistic assumption on subset size (i.e., JT-CoMP, $L = B$) can provide higher instantaneous SINR (4), but it is more susceptible to the outage with the slight increase in blockage probability. Moreover, these outage events will eventually increase the queue-backlogs (39), i.e., due to unsuccessful data transmissions. Thus, to guarantee the average latency requirements (9b), the network consumes more power, and attempts to increase the achievable rates during potentially unblocked events. Thus, it results in a lower sum-power performance with increasing blockage, as shown in Fig. 9. Furthermore, our proposed dynamic choice of serving set size ensures the same average latency requirements with minimum sum-power, and efficiently adopts with the uncertainties of mmWave radio channel and unpredictable blockage events. Note that the resulting gap in the dynamic subset selection relative to the lower envelope is mainly due to the limited and discrete choices of parameter L , and the approximation error of the time-averaged blockage in (37), as also illustrated in Fig. 7.

Fig. 10 illustrates the trade-offs between rates and reliable connectivity with parameter $V = 1$ and blockage $q = 10\%$.

However, similar behavior can be observed for different parameter settings, which is not included due to space limitations. It can be concluded from Fig. 10 that the outage is decreased from 35% to less than 0.5% by changing parameter L from 4 (full JT-CoMP) to 2 (proposed), in problem (9). Thus, the pessimistic SINR estimate over the link blockage combinations greatly improves the outage performance. Clearly, there is a trade-off between reliable connectivity, rate, and sum-power performance. More specifically, for a given queue length (i.e., latency requirements), we can guarantee a user-rate with minimum sum-power and vice-versa. However, compared to the baseline schemes, the proposed method provides power-efficient, high-reliability, and low-latency mmWave communication.

VII. CONCLUSION

In this paper, we have studied the trade-off between reliable downlink transmission and sum-power performance in a mmWave based dynamic systems, by exploiting the multi-antenna spatial diversity and CoMP connectivity. We considered a time-average sum-power minimization problem subject to maximum allowable queue length constraint. We have adapted the Lyapunov optimization framework, and derived a dynamic control algorithm for the long-term time-average stochastic problem. We proposed a robust transmit beamformer design by considering a pessimistic estimate of rates and a proactive selection of the serving set combinations of available CoMP RRUs. Furthermore, the non-convex and coupled constraints are handled using FP techniques. The closed-form algorithm is provided by iteratively solving a system of KKT optimality conditions, while accounting for the uncertainties of mmWave radio channel. The numerical results manifested the robustness of the proposed beamformer design in the presence of random link blockages. Specifically, the achievable rate and sum-power performance with our proposed method outperforms the baseline scenarios while ensuring user-specific latency requirements, and results in power-efficient, highly-reliable, and low-latency mmWave communication.

REFERENCES

- [1] D. Kumar, S. K. Joshi, and A. Tölli, "Latency-aware reliable mmwave communication via multi-point connectivity," in *Proc. IEEE Global Commun. Conf.*, 2020, pp. 1–6.
- [2] W. Saad, M. Bennis, and M. Chen, "A vision of 6G wireless systems: Applications, trends, technologies, and open research problems," *IEEE Network*, vol. 34, no. 3, pp. 134–142, 2020.
- [3] G. R. MacCartney, T. S. Rappaport, and S. Rangan, "Rapid fading due to human blockage in pedestrian crowds at 5G millimeter-wave frequencies," in *Proc. IEEE Global Commun. Conf.*, Dec. 2017.
- [4] C. Slezak, V. Semkin, S. Andreev, Y. Koucheryavy, and S. Rangan, "Empirical effects of dynamic human-body blockage in 60 GHz communications," *IEEE Commun. Mag.*, vol. 56, no. 12, pp. 60–66, 2018.
- [5] H. Shariatmadari, Z. Li, M. A. Uusitalo, S. Iraj, and R. Jäntti, "Link adaptation design for ultra-reliable communications," in *Proc. IEEE Int. Conf. Commun.*, May 2016, pp. 1–5.
- [6] D. Kumar, J. Kaleva, and A. Tölli, "Blockage-aware reliable mmWave access via coordinated multi-point connectivity," *IEEE Trans. Wireless Commun.*, pp. 1–1, 2021.
- [7] J. Kaleva, A. Tölli, M. Juntti, R. A. Berry, and M. L. Honig, "Decentralized joint precoding with pilot-aided beamformer estimation," *IEEE Trans. Signal Process.*, vol. 66, no. 9, pp. 2330–2341, May 2018.
- [8] 3GPP TSG RAN Meeting #82, TS 37.340, "NR; Multi-connectivity; Overall description (Release 15)," Rel. 15, Jun 2018.
- [9] Qualcomm, "How CoMP can extend 5G NR to high capacity and ultra-reliable communications," <https://www.qualcomm.com/documents/how-comp-can-extend-5g-nr-high-capacity-and-ultra-reliable-communications>, [Online] Accessed: 2021-04-22.
- [10] A. Tölli, H. Pannanen, and P. Komulainen, "On the value of coherent and coordinated multi-cell transmission," in *Proc. IEEE Int. Conf. Commun. Workshop*, Jun. 2009, pp. 1–5.
- [11] R. Irmer *et al.*, "Coordinated multipoint: Concepts, performance, and field trial results," *IEEE Commun. Mag.*, vol. 49, no. 2, pp. 102–111, Feb. 2011.
- [12] G. Nigam, P. Minero, and M. Haenggi, "Coordinated multipoint joint transmission in heterogeneous networks," *IEEE Trans. Commun.*, vol. 62, no. 11, pp. 4134–4146, Nov. 2014.
- [13] G. R. MacCartney and T. S. Rappaport, "Millimeter-wave base station diversity for 5G coordinated multipoint (CoMP) applications," *IEEE Trans. Wireless Commun.*, vol. 18, no. 7, pp. 3395–3410, Jul. 2019.
- [14] D. Maamari, N. Devroye, and D. Tuninetti, "Coverage in mmWave cellular networks with base station co-operation," *IEEE Trans. Wireless Commun.*, vol. 15, no. 4, pp. 2981–2994, Apr. 2016.
- [15] M. Gerasimenko, D. Moltchanov, M. Gapeyenko, S. Andreev, and Y. Koucheryavy, "Capacity of multiconnectivity mmWave systems with dynamic blockage and directional antennas," *IEEE Trans. Veh. Technol.*, vol. 68, no. 4, pp. 3534–3549, 2019.
- [16] M. Gapeyenko, V. Petrov, D. Moltchanov, M. R. Akdeniz, S. Andreev, N. Himayat, and Y. Koucheryavy, "On the degree of multi-connectivity in 5G millimeter-wave cellular urban deployments," *IEEE Trans. Veh. Technol.*, vol. 68, no. 2, pp. 1973–1978, 2019.
- [17] S. R. Khosravirad and H. Viswanathan, "Analysis of feedback error in automatic repeat request," *CoRR*, vol. abs/1710.00649, 2017. [Online]. Available: <http://arxiv.org/abs/1710.00649>
- [18] Z. Ma, M. Xiao, Y. Xiao, Z. Pang, H. V. Poor, and B. Vucetic, "High-reliability and low-latency wireless communication for internet of things: Challenges, fundamentals, and enabling technologies," *IEEE Internet Things J.*, vol. 6, no. 5, pp. 7946–7970, 2019.
- [19] M. J. Neely, *Stochastic Network Optimization with Application to Communication and Queueing Systems*, ser. Synthesis Lectures on Communication Networks. Morgan & Claypool, 2010, vol. 7.
- [20] K. Shen and W. Yu, "Fractional programming for communication systems—part I: Power control and beamforming," *IEEE Trans. Signal Process.*, vol. 66, no. 10, pp. 2616–2630, 2018.
- [21] A. Beck, A. Ben-Tal, and L. Tetrushvili, "A sequential parametric convex approximation method with applications to nonconvex truss topology design problems," *J. Global Optim., Springer*, vol. 47, no. 1, pp. 29–51, 2010.
- [22] T. Bai, R. Vaze, and R. W. Heath, "Analysis of blockage effects on urban cellular networks," *IEEE Trans. Wireless Commun.*, vol. 13, no. 9, pp. 5070–5083, 2014.
- [23] M. Di Renzo, "Stochastic geometry modeling and analysis of multi-tier millimeter wave cellular networks," *IEEE Trans. Wireless Commun.*, vol. 14, no. 9, pp. 5038–5057, Sep. 2015.
- [24] E. Hriba and M. C. Valenti, "The potential gains of macrodiversity in mmWave cellular networks with correlated blocking," in *Proc. IEEE Military Commun. Conf.*, 2019, pp. 171–176.
- [25] A. Checko, H. L. Christiansen, Y. Yan, L. Scolari, G. Kardaras, M. S. Berger, and L. Dittmann, "Cloud RAN for mobile networks—a technology overview," *IEEE Commun. Surveys Tuts.*, vol. 17, no. 1, pp. 405–426, Firstquarter 2015.
- [26] D. Gross, J. F. Shortle, J. M. Thompson, and C. M. Harris, *Fundamentals of queueing theory*. John Wiley & Sons, 2008.
- [27] K. Shen and W. Yu, "Fractional programming for communication systems—part II: Uplink scheduling via matching," *IEEE Trans. Signal Process.*, vol. 66, no. 10, pp. 2631–2644, 2018.
- [28] Q. Chen, K. Yang, H. Jiang, and M. Qiu, "Joint beamforming coordination and user selection for CoMP enabled NR-U networks," *IEEE Internet Things J.*, pp. 1–1, 2021.
- [29] M. Grant and S. Boyd, "CVX: Matlab software for disciplined convex programming, version 2.1," <http://cvxr.com/cvx>, Mar. 2014.
- [30] S. Boyd and L. Vandenberghe, *Convex optimization*. Cambridge university press, 2004.
- [31] S. Boyd, L. Xiao, and A. Mutapcic, "Subgradient methods," *lecture notes of EE392o, Stanford University*, 2003.
- [32] M. S. Lobo, L. Vandenberghe, S. Boyd, and H. Lebet, "Applications of second-order cone programming," *Linear Algebra and Applications*, vol. 284, pp. 193–228, Nov. 1998.
- [33] A. M. Sayeed, "Deconstructing multiantenna fading channels," *IEEE Trans. Signal Process.*, vol. 50, no. 10, pp. 2563–2579, 2002.